ISPRS Journal of Photogrammetry and Remote Sensing 87 (2014) 57–67

Contents lists available at ScienceDirect

ISPRS Journal of Photogrammetry and Remote Sensing

journal homepage: www.elsevier.com/locate/isprsjprs

EarthEnv-DEM90: A nearly-global, void-free, multi-scale smoothed, 90m digital elevation model from fused ASTER and SRTM data

Natalie Robinson [a,*], James Regetz [b], Robert P. Guralnick [a]

[a] University of Colorado Museum and Department of Ecology and Evolutionary Biology, UCB 334, University of Colorado, Boulder, CO 80309-0334, USA
[b] National Center for Ecological Analysis and Synthesis, 735 State Street, Suite 300, Santa Barbara, CA 93101, USA

ARTICLE INFO

Article history:
Received 28 May 2013
Received in revised form 30 October 2013
Accepted 1 November 2013
Available online 28 November 2013

Keywords:
Global Digital Elevation Model (DEM)
Void-filling
Multi-scale smoothing
SRTM
ASTER
DEM blending

ABSTRACT

A variety of DEM products are available to the public at no cost, though all are characterized by trade-offs in spatial coverage, data resolution, and quality. The absence of a high-resolution, high-quality, well-described and vetted, free, global consensus product was the impetus for the creation of a new DEM product described here, 'EarthEnv-DEM90'. This new DEM is a compilation dataset constructed via rigorous techniques by which ASTER GDEM2 and CGIAR-CSI v4.1 products were fused into a quality-enhanced, consistent grid of elevation estimates that spans ~91% of the globe. EarthEnv-DEM90 was assembled using methods for seamlessly merging input datasets, thoroughly filling voids, and smoothing data irregularities (e.g. those caused by DEM noise) from the approximated surface. The result is a DEM product in which elevational artifacts are strongly mitigated from the input data fusion zone, substantial voids are filled in the northern-most regions of the globe, and the entire DEM exhibits reduced terrain noise. As important as the final product is a well defined methodology, along with new processing techniques and careful attention to final outputs, that extends the value and usability of the work beyond just this single product. Finally, we outline EarthEnv-DEM90 acquisition instructions and metadata availability, so that researchers can obtain this high-resolution, high-quality, nearly-global new DEM product for the study of wide-ranging global phenomena.
© 2013 International Society for Photogrammetry and Remote Sensing, Inc. (ISPRS) Published by Elsevier B.V. All rights reserved.

1. Introduction

Digital Elevation Models (DEMs) are grids containing regularly spaced elevation values, typically based on remote sensing measurements. A variety of DEM products are freely available to the public, all of which exhibit advantages and drawbacks with regard to spatial coverage, data resolution, and quality. Quality differences, including localized issues such as missing values or prominent spikes and wells, and more systematic problems such as striped or noisy outputs (Fisher and Tate, 2006; Gallant, 2011), are particularly problematic for researchers who must assemble multiple DEMs in order to analyze terrain-based phenomena across broad spatial extents. Such data assembly and merging, using incongruent datasets of inconsistent quality, may be prohibitively difficult for those who have limited time or experience in working with spatial data. In these cases, researchers may be constrained to working with data that are lower quality and/or coarser resolution than desired. There is a need for a global, high-resolution, consensus DEM product that fills the current data gap and provides consistent information toward increasingly global-scale monitoring and analyses.

The most quality-controlled, broadest coverage DEM currently available is published by the Consortium for Spatial Information of the Consultative Group of International Agricultural Research (CGIAR-CSI), and is a post-processed derivative of the Shuttle Radar Topography Mission (SRTM) (Hong et al., 2006; Nikolakopoulos et al., 2007). The most recent version of this high-resolution (~90 m) product is CGIAR-CSI SRTM v4.1 (Jarvis et al., 2008), which was created after several iterations of processing on SRTM version 2 (Section 2.1.2). Unfortunately, CGIAR-CSI SRTM v4.1 coverage is not global, as no data exist for regions north of N60 (including much of Russia, Canada, Alaska and the Nordic countries) and south of S60 (Antarctica). In these regions, the very-high resolution (~30 m) Advanced Spaceborne Thermal Emission and Reflection Radiometer (ASTER) Global Digital Elevation Model (GDEM) version 2 is available. However, ASTER GDEM2 is characterized by extensive voids throughout the dataset, particularly at high and low latitudes (>N60 and <S60, Tachikawa et al., 2011; Urai et al., 2012). Such data deficiency strongly impacts the derivation of second-order products like slope and aspect grids (Franklin, 1995), leading to faulty calculations unless these gaps are repaired. Since the onus for such repairs is on the individual end user, this may

* Corresponding author. Tel.: +1 303 588 1689.
E-mail address: n.robinson@colorado.edu (N. Robinson).

0924-2716/$ - see front matter © 2013 International Society for Photogrammetry and Remote Sensing, Inc. (ISPRS) Published by Elsevier B.V. All rights reserved.
http://dx.doi.org/10.1016/j.isprsjprs.2013.11.002

result in duplicated efforts and, depending on methodologies employed, inconsistent downstream results. All other freely available DEMs that are global in coverage are of a minimum 7.5 arc-sec (~250 m) resolution, and are thus too coarse for use in many applications.

The absence of a high-resolution, high-quality, free, global consensus product was the impetus for the creation of a new DEM product described here, 'EarthEnv-DEM90'. This new high resolution DEM has been carefully constructed from the highest quality free DEMs that could be obtained for different areas of the globe. EarthEnv-DEM90 was assembled using rigorous techniques for: (1) combining incongruous datasets, due to differences in sensor technologies and/or methodologies used to convert sensor data into final DEM products (Schindler et al., 2011), and (2) repairing data quality issues in both the input DEMs and resulting consensus product. Specifically, DEMs with incompatible overlapping values were seamlessly merged in order to eliminate elevational cliffs that resulted in the absence of blending across the transition zone. In addition, a thoroughly tested void-filling technique was used to improve ASTER GDEM2 products. Finally, an adaptive multi-scale smoothing algorithm (Gallant, 2011) was applied over the entire spatial extent of the DEM in order to reduce data irregularities, such as those caused by DEM noise, from the approximated surface. Together, these techniques result in a DEM product that is useful for researchers wishing to evaluate wide-ranging terrain-based phenomena, and that has been made available to the scientific community at no cost and with the appropriate metadata. Here, we describe the assembly process for EarthEnv-DEM90, as well as dataset acquisition instructions and metadata availability.

2. Materials and methods

2.1. Input data

EarthEnv-DEM90 comprises three freely-available input datasets: 1 arc-sec (~30 m) ASTER GDEM2, 3 arc-sec (~90 m) CGIAR-CSI SRTM v4.1, and 3 arc-sec GLSDEM. All input datasets were obtained in un-projected, WGS84 geodetic datum, and specifications for each dataset are as follows:

2.1.1. ASTER GDEM2

The ASTER mission is a joint project between the National Aeronautics and Space Administration (NASA) and the Ministry of Economy, Trade and Industry (METI). Elevations were measured aboard NASA's Terra Satellite, beginning in 1999, using downward and rearward pointing stereoscopic cameras. These cameras captured overlapping near-infrared images of effectively global geographic extent (latitudes S83 to N83). In 2011, a second data product was introduced in which the original data were: (1) augmented with an additional 260,000 overlapping images, and (2) refined in order to decrease the incidence of data artifacts, improve the spatial resolution, and increase the accuracy of water body coverage (http://asterweb.jpl.nasa.gov/gdem.asp, 2013). The resulting DEM (NASA, 2011) has an average vertical accuracy of −0.2 m, when compared to ~18,000 geodetic references points occurring over the Conterminous US (CONUS), and an accuracy of 17 m at the 95% confidence level (Tachikawa et al., 2011). Average horizontal displacement for ASTER GDEM2 is approximately 0.23 pixels, and horizontal resolution is comparable to that of SRTM data (Tachikawa et al., 2011).

Despite the advantageous qualities of ASTER GDEM2, namely its global coverage and generally high vertical and horizontal accuracy, the dataset is also characterized by a variety of artifacts and anomalies that make its use problematic without further processing. One such issue arises from fact that elevations are measured from Earth's reflective surface, including dense forest canopies or buildings (Gesch et al., 2011). As a result, the accuracy of ASTER GDEM2 measurements are particularly sensitive to land cover, and are lower for forested than open or bare areas (Tachikawa et al., 2011; Gesch et al., 2011). In addition, ASTER GDEM2 contains numerous voids at high latitudes (above N60) due to the replacement of spikes and wells with null data (Tachikawa et al., 2011), and at low latitudes (below S60) due to snow and cloud interference (Urai et al., 2012).

ASTER GDEM2 data were downloaded in 1° × 1° tiles, from the NASA Land Processes Distributed Active Archive Center (LP DAAC) and using the Reverb data discovery tool (http://reverb.echo.nasa.gov/reverb, 2011).

2.1.2. CGIAR-CSI SRTM v4.1

The SRTM dataset represents a collaborative effort between NASA and the National Geospatial Intelligence Agency (NGA). Data were collected over an 11-day mission in February 2000, aboard the Space Shuttle Endeavor, and are available for ~80% of the globe (up to 60° north and south). Elevations were measured via radar interferometry, using an onboard/outboard antenna system and single-pass data acquisition. Since its original release, SRTM has been updated multiple times in order to remove erroneous pixel values (spikes and wells), better delineate water body boundaries, fill data voids, etc. Edits to the original dataset were performed by NGA, and the current NASA-SRTM release is v2.1 (Farr et al., 2007; http://dds.cr.usgs.gov/srtm/What_are_these.pdf, 2013). Accuracy assessments of the DEM's elevational measurements, compared to ground-collected global positioning system (GPS) control points, have returned average vertical errors of −0.7 to 1.8 m among six different continents, with ranges of 6–10 m at the 90% confidence level (Rodriguez et al., 2005). As seen for ASTER GDEM2 data, vertical accuracy is influenced by land cover (see Section 2.1.1), though this is less problematic for SRTM data because elevational measurements partially penetrate forest canopies (Gesch et al., 2011). Finally, over the same six continents examined in vertical accuracy assessments, average horizontal accuracy ranged from 9.0 to 11.9 m (Rodriguez et al., 2005).

Since its release, SRTM v2 has been subjected to multiple rounds of processing by CGIAR-CSI (Jarvis et al., 2008). These have resulted in the most recent SRTM product, CGIAR-CSI SRTM v4.1. Together, the repeated data improvement efforts and rigorous quality control of the SRTM products has made CGIAR-CSI SRTM v4.1 a highly trusted and widely used data product. While accuracy assessments indicate that this DEM provides more accurate elevational measurements than does ASTER GDEM2, the biggest limitation of the dataset is that it does not cover regions in northern latitudes (above N60), and is thus not a truly global product.

CGIAR-CSI SRTM v4.1 data were downloaded in 5° × 5° tiles, from CGIAR-CSI (http://srtm.csi.cgiar.org/SELECTION/inputCoord.asp, 2011).

2.1.3. GLSDEM

GLSDEM (USGS, 2008) is a 3 arc-sec compilation dataset produce by the Global Land Cover Facility (GLCF). The dataset contains inputs from several public and commercial products that vary in resolution and quality (http://www.glcf.umd.edu/data/glsdem/description.shtml, 2013). These input DEMs were resampled where necessary (Global Land Survey Digital Elevation Model (GLSDEM) Technical Guide), and merged into a global product. Rigorous data merging techniques were not applied during the compilation of GLSDEM, as this was not the motivation for its construction. As GLSDEM was only used as an ancillary dataset to help fill voids in high latitude ASTER GDEM2 (Section 2.2.1), accuracy and quality of GLSDEM are not discussed here as they were in Sections 2.1.1 and 2.1.2. GLSDEM data were downloaded in 1° × 1° tiles from

the GLCF database, via file transfer protocol (ftp://ftp.glcf.umd.edu/glcf/GLSDEM/, 2012).

2.2. DEM processing and assembly

Data processing for EarthEnv-DEM90 was performed in three zones, based on input data availability and quality. All methods were carried out using open-source programs including the Geospatial Data Abstraction Library (GDAL), GRASS 7.0 (http://grass.osgeo.org/), Quantum GIS (QGIS, http://www.qgis.org/), R (http://www.r-project.org), and Python (http://www.python.org). Data zones and processing methods are shown diagrammatically in Fig. 1 and are as follows:

2.2.1. ASTER zone

The ASTER data zone (Fig. 1A) spans latitudes N59 to N83, in accordance with ASTER GDEM2 data availability in the northernmost reaches of the globe. We first used bilinear resampling to aggregate ASTER GDEM2 data to 3 arc-sec resolution, and to shift grids ½ pixel in the *x* and *y*-directions. This aligned cell edges, as opposed to centers, with exact degree lines. It also eliminated boundary overlap between adjacent tiles, the need for which arose from numerous instances of pixel mismatch where raw ASTER GDEM2 tiles overlapped. Resampled tiles were then mosaicked into one inclusive DEM.

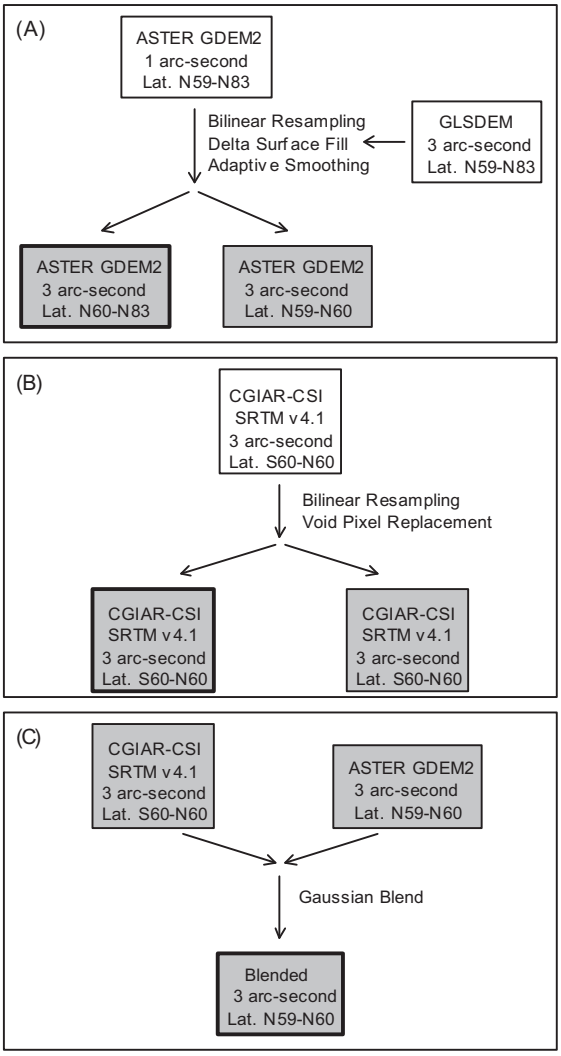

Fig. 1. Data processing methods used in each of the ASTER (A), SRTM (B), and the blend zones (C). Raw input data are represented by white boxes, and processed data by grey boxes. Boxes with heavy black borders represent input data for EarthEnv-DEM90.

While processing the ASTER GDEM2 dataset, we encountered numerous voids, predominantly in the eastern hemisphere. These constituted almost 43 million pixels (~1% of pixels in tiles where they occurred, and ~350 million km^2 of total landmass) for which data had not been collected by the remote sensing instrumentation or, more frequently, anomalous elevational values had been removed during processing (Section 2.1.1). We filled these voids using the Delta Surface Fill (DSF) method (Grohman et al., 2006; Fig. 2). Here, the average vertical distance between the void-prone DEM and corresponding pixels in an ancillary dataset (in this case GLSDEM) is inserted into the centers of large voids. Remaining void pixels are then estimated through standard interpolation, where the algorithm is informed by both the true vertical differences between datasets, at the void interface, as well as the average vertical difference of two DEMs, at the void center. This method results in more accurate estimates than those generated by traditional void-filling approaches alone (Grohman et al., 2006).

Before performing void-filling, we first isolated the region of the resampled ASTER GDEM2 DEM which contained voids, and clipped it into 72 equally sized tiles of 10° × 11.5° (longitude by latitude). We then acquired GLSDEM tiles for use as the ancillary dataset, and applied bilinear resampling to align them with ASTER GDEM2 tiles. These data were then mosaicked into 10° × 11.5° (longitude × latitude) tiles that corresponded with ASTER GDEM2 tiles. Each GLSDEM/ASTER GDEM2 grid pair (Fig. 2A) was next used to create a 'delta surface' of the differences between corresponding pixels in the grids. Null pixels were passed through to the delta surface such that it contained the same voids as ASTER GDEM2 (Fig. 2B). The average value for the entire delta surface was then inserted into the centers of 11 × 11 pixel voids. This void size is somewhat larger than that suggested by Grohman et al. (2006), but was more computationally feasible, given the vast extent over which void filling was required. The remaining void pixels were then filled using regularized spline with tension (rst) interpolation (Fig. 2C). This method uses a function through which deviations from both

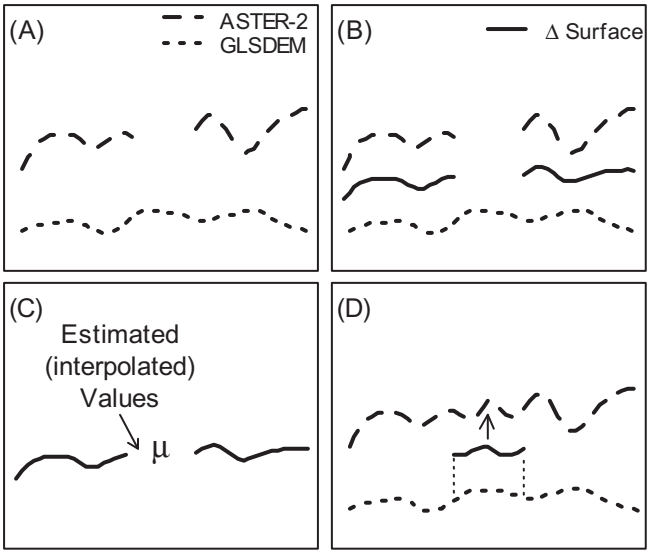

Fig. 2. Delta Surface Fill (DSF) method. ASTER GDEM2 and GLSDEM input data (A) are first subtracted to create a delta surface which contains voids native to ASTER GDEM2 (B). The mean delta value is then inserted into the center of voids in the delta surface, and surrounding pixel values estimated through interpolation (C). Finally, the estimated pixel values are added back to the GLSDEM, and the results combined with ASTER GDEM2 for a void-filled surface (D). Figure is adapted from Grohman et al., 2006.

given data points and the smoothness seminorm are minimized during interpolation, and is equivalent to interpolation by universal kriging using a covariance function that is determined by the smoothness of the seminorm (Mitasova et al., 2005). Further detail regarding the rst method, including theory and equations, can be found in Mitasova and Mitas (1993). The algorithm was chosen due to its proficiency in filling voids of varying sizes that lie in relatively variable terrain (Hofierka et al., 2002; http://srtm.csi.cgiar.org/SRTMdataProcessingMethodology.asp, 2013). Finally, the void-filled delta surface was added back to GLSDEM in order to obtain pixel estimates within the voids, and these estimated values inserted into voids in the ASTER GDEM2 tiles (Fig. 2D). Calculations were performed using the r.fillnulls function in GRASS.

Before performing rst interpolation, we were first required to specify tension and smoothing parameters for the algorithm. These related parameters control the relative shape and structure of the interpolated surface. Tension influences the surface's level of detail (Mitasova et al., 2005), where a high tension parameter results in a membrane-like surface that follows data point trends, while low tension results in a rigid plate-like surface which overshoots some of the data points (Hargrove, 1995; Mitasova et al., 2005; Fig. 3A). Smoothing affects the vertical deviation between the data points and the surface itself (Mitasova et al., 2005), where the surface is forced to pass through the data points when the smoothing parameter is set to 0 (which may result in puckering or distortion of the surface) while being allowed to deviate from the data points when set at higher values (Hargrove, 1995; Fig. 3B). Because we were applying interpolation over a large extent, in which terrain varied greatly, we could not assume that the default smoothing and tension settings (in r.fillnulls) were appropriate for our needs. Thus, we performed a series of best fit analyses, over multiple test regions, in which data estimated using combinations of tension and smoothing parameters were compared to actual DEM values in order to identify the parameter combination through which those values were most accurately estimated over a broad spatial extent. Analyses were performed in areas where terrain was both relatively flat (North-central Canada) and more mountainous (Eastern Russia and Northwestern Canada), and were conducted as follows:

(A) Voids in the Eastern Russia test region were shifted 100 pixels directly to the east in order to create 'simulated voids' of the same size and shape, but with underlying data to which estimated pixel values could be compared.
(B) Using default tension and smoothing parameters (40 and 0.1, respectively), we performed rst interpolation to estimate pixel values within the simulated voids. Results were compared to actual values underlying the simulated voids, on a pixel-to-pixel basis. Comparisons included: (a) the percentage of shared values (i.e. the number of times interpolation correctly estimated a pixel value), (b) correlation, and (c) root mean square error (RMSE) of the differences between actual and interpolated values. All statistical analyses were performed in Python.
(C) Tension was then increased by increments of 5, and pixel estimates again compared with actual data. This was repeated until statistical outputs were similar enough to be considered equivalent. For each of the tension levels, comparisons were also analyzed for smoothing parameters of 0.001, 0.01, 0.5, 0.6 and 0.7.
(D) The above analyses were repeated for the two Canadian test regions, using Eastern Russia voids that were burned into these otherwise void-free areas. We then compared all results, in order to identify parameter values that maximized null pixel estimation accuracy across all regions.

As a final quality assurance measure, we compared pixel estimates calculated from spline interpolation alone to those calculated using the DSF method. This was performed over the North-central Canada test region, with spline tension and smoothing parameters set to the best values established above. Results suggested that the DSF method performed better than spline interpolation alone (Section 3.1), so the DSF method was then used to fill voids over the entire ASTER GDEM2 region of EarthEnv-DEM90. Void-filling was performed as-needed for the $10^\circ \times 11.5^\circ$ ASTER GDEM2 tiles, and the resulting tiles then mosaicked into one inclusive DEM for latitudes N60 to N83. Finally, void-filled ASTER GDEM2 tiles were clipped into $5^\circ \times 5^\circ$ (or $5^\circ \times 3^\circ$ (longitude $\times$ latitude), at N80 to N83) extents for co-registration with CGIAR-CSI SRTM v4.1 tile extents. In addition, $5^\circ \times 1^\circ$ tiles were generated for the ASTER GDEM2 data occurring between latitudes of N59 and N60 (the blend zone, Section 2.2.4).

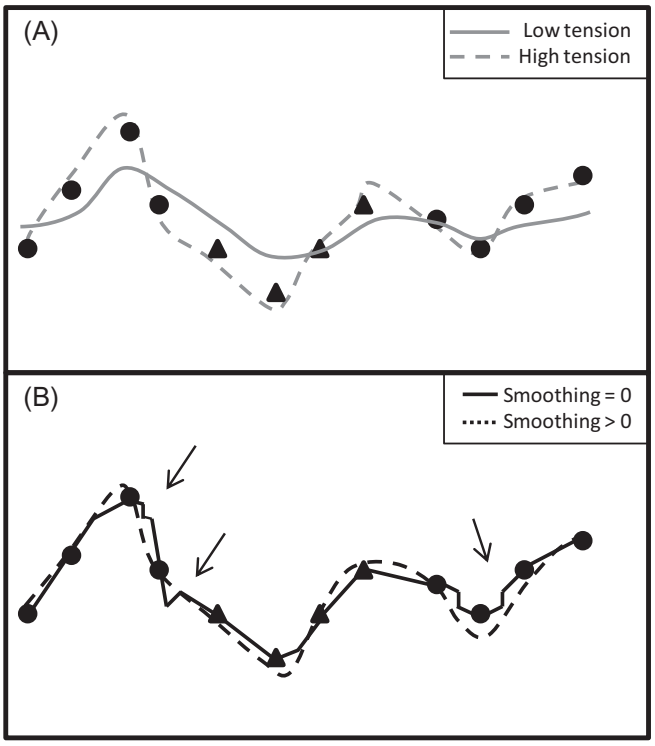

Fig. 3. Conceptual explanation of the influences of tension and smoothing parameters on interpolated surfaces using the regularized spline with tension (rst) method. The tension parameter (A) tunes the character of the surface from membrane-like (high tension) to rigid plate-like (low tension). The smoothing parameter (B) controls the allowed deviance of the surface from data points in the DEM, where setting the smoothing to 0 forces the surface to pass through data points and may result in distortions in the interpolated surface (arrows). Actual data points are represented by black dots, and interpolated points by black triangles (here representing estimated points to fill a large void).

2.2.2. SRTM zone

The SRTM zone (Fig. 1B) spans latitudes S60 to N60. Processing of CGIAR-CSI SRTM v4.1 data began with bilinear resampling of each $5^\circ \times 5^\circ$ tile into a new grid, shifted by ½ pixel in the *x* and *y*-directions, in order to co-register the tiles with those of ASTER GDEM2. CGIAR-CSI SRTM v4.1 tiles were next inspected for any voids that may have remained following CGIAR-CSI data processing. We found four tiles containing voids that were surrounded by large regions of identical and equal pixels. Because these voids were clearly anomalous occurrences in otherwise flat areas, we filled them with the values of the surrounding pixels using a simple mapcalc function in GRASS. All resampled CGIAR-CSI SRTM v4.1

tiles were then mosaicked into one inclusive DEM. Where no CGIAR-CSI SRTM v4.1 tile existed (regions with no landmass), we filled pixels with a value of zero. Finally, CGIAR-CSI SRTM v4.1 ocean pixels were reclassified from null to zero so that all ocean pixels within EarthEnv-DEM90 contained a value of zero.

2.2.3. DEM smoothing

Following ASTER GDEM2 and CGIAR-CSI SRTM v4.1 data processing, we post-processed all tiles using an adaptive, multi-scale smoothing technique (Fig. 4). This helped to reduce noise in the output EarthEnv-DEM90 data. Such methods are particularly important in densely sampled DEM datasets such as ASTER GDEM2 and CGIAR-CSI SRTM v4.1, and multi-scale smoothing is well-suited for this purpose because the level of smoothing is adaptive to the amount of noise in the dataset (smoothing is applied aggressively when noise is large relative to topographic variation, and little to not at all when the converse is true (Gallant, 2011)). Technical underpinnings for this procedure can be found in Gallant (2011). This author kindly provided initial scripts for the multi-scale smoothing work performed here, with adaptations made to these scripts in order to handle global data that included terrain occurring at coastlines.

Multi-scale smoothing was performed in GRASS, via Python scripts. The two-step process first involved the derivation of a standard deviation grid in order to help quantify 'noise' in the input DEM. Here, a mean was calculated for a neighborhood surrounding each pixel of interest, and the difference between the pixel value and neighborhood mean computed. Next, the standard deviation of these differences was calculated over a 5-pixel neighborhood, and this value inserted into the pixel of interest in the resulting noise grid. This noise grid was then used to adaptively smooth the input DEM. This first involved the calculation of a mean and variance for cells within a circular neighborhood surrounding each pixel of interest (Fig. 4A), where variance was the square of the corresponding pixel value in the standard deviation grid. This was repeated for consecutively larger neighborhoods (coarser resolution grids, Fig. 4B). As coarser resolution statistics were calculated, they were compared with those of the previous (finer) resolution neighborhood and used to calculate an adjusted overall mean and variance for that finer resolution. Thus the overall mean and variance at each resolution reflected terrain stochasticity across two scales. Lastly, the variances and means were recombined for coarser and finer resolutions in a reverse sequence. This required that the coarsest resolution mean and variance grid first be refined (disaggregated) back to the previous resolution. This refined grid was then recombined with the previous resolution mean and variance grid to obtain 'smoothed' mean and variance values at the finer resolution (Fig. 4C). These values now reflected terrain variation across three scales, those of the resolution in question as well as finer and coarser resolutions. Finally, the smoothed means and variances at the original DEM resolution were used to calculate smoothed elevation values (the smoothed DEM) for this resolution (Fig. 4D). More details are available in Gallant (2011).

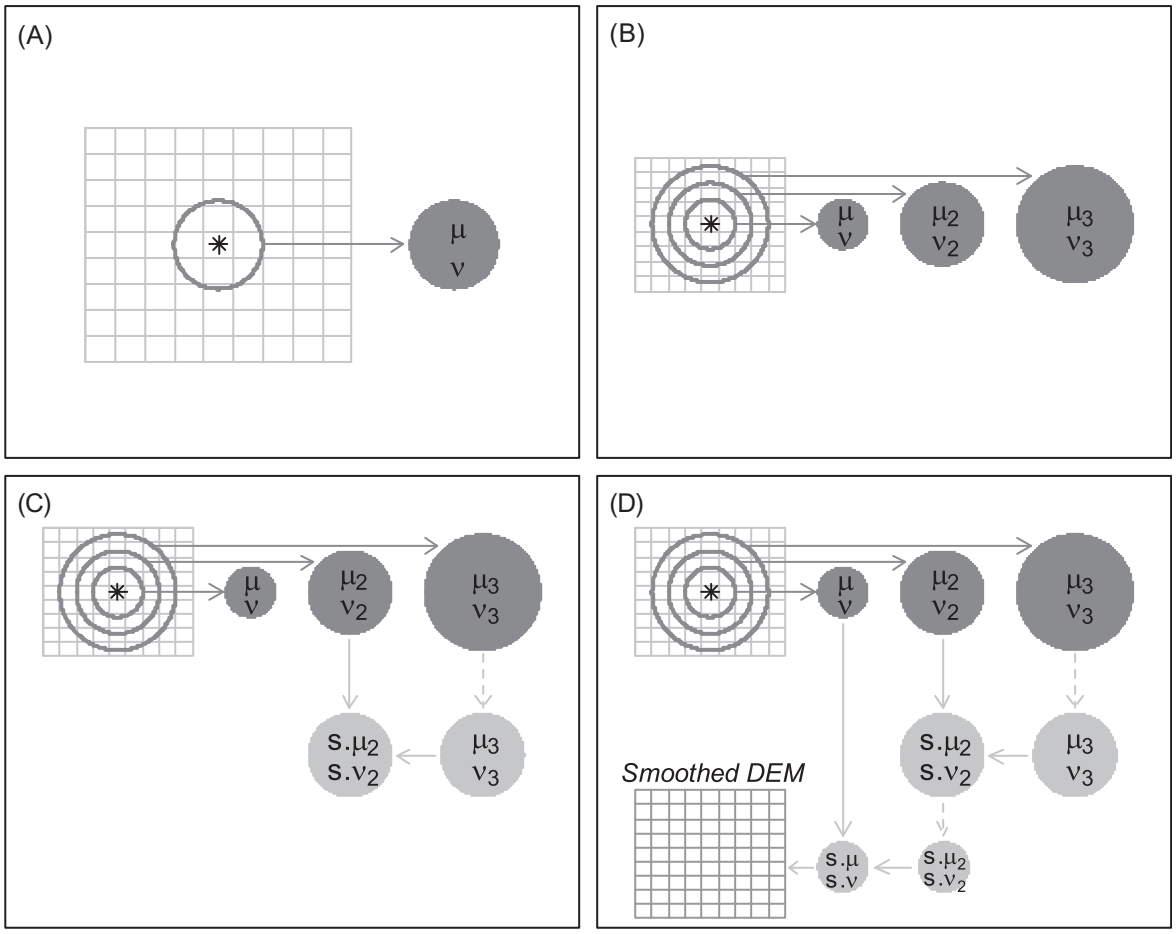

Fig. 4. Adaptive multi-scale smoothing method. A mean (μ) and variance (ν) are first calculated within a neighborhood surrounding a pixel of interest (*) in the input DEM (A), and this is repeated for consecutively larger neighborhoods (B). The coarsest resolution grid is then disaggregated to the previous resolution (dashed arrow), and this grid is recombined with the overall mean and variance from the previous resolution grid in order to obtain a smoothed mean (s. μ) and variance (s. ν) (C). This is repeated at consecutively finer resolutions until the initial resolution is reached, and smoothed elevation values are calculated (D).

It should be noted that we performed one additional step to those described in Gallant (2011) during multi-scale smoothing. This involved resetting all output pixels for which the value in the input DEM was zero back to that value, in both the standard deviation grid (prior to smoothing) as well as the smoothed grid. In this way, we eliminated variance values that were calculated for ocean pixels occurring near coastal terrain, and the subsequent influence that they would have on this terrain during smoothing. Multi-scale smoothing was performed on processed ASTER GDEM2 and CGIAR-CSI SRTM v4.1 tiles (Sections 2.2.1 and 2.2.2), but with an extra 100 buffer pixels around each edge. These pixels were removed from the tiles following adaptive smoothing, thereby eliminating edge-effects from the smoothed DEM. For tiles occurring at the true edges of the ASTER GDEM2 (latitudes N59 and N83) and CGIAR-CSI SRTM v4.1 (latitudes S60 and N60) datasets, the top or bottom 100 rows of pixels were inverted and added to the true edge in order to create this 100 pixel buffer.

2.2.4. Blend zone

The blend zone (Fig. 1C) corresponds to the area of overlap between ASTER GDEM2 and CGIAR-CSI SRTM v4.1 data, at latitudes N59 to N60. Before blending these DEMs, we tested whether we could simply join the two layers and the N60 transition line. We used non-smoothed input ASTER GDEM2 and CGIAR-CSI SRTM v4.1 data for these tests, in order to broadly evaluate 'best blending practices'. We focused on a small region in Canada (latitudes N59.875 to N60.125, longitudes W136 to W96), and compared latitudinal profiles of: (a) mean elevation (in meters), (b) slope (in degrees), (c) circular aspect (angular direction in degrees), and (d) single flow direction, for each of the two DEMs. This last measure was computed for a subset of the data, with the same latitudinal extents but from longitudes W125 to W100, due to computational limitations. The results of this analysis (Section 3.3) suggested that proper fusion of the two datasets required a different approach than simply fusing the data.

We then investigated DEM blending via different techniques for calculating weighted averages of ASTER GDEM2 and CGIAR-CSI SRTM v4.1 for each pixel approaching the N60 transition line. We tested four methods, each of which used a separate algorithm to estimate relative DEM contributions at each pixel in the test region. These included an exponentially declining predictive model, a local regression (LOESS) predictive model, Burt and Adelson's (1983) multiresolution spline method, and Gaussian weighted averaging (hereafter 'Gaussian'). For each blending method, we again generated latitudinal profiles for mean elevation, slope, aspect and flow direction over the test region described above. Because these profiles were based on latitudinal means, the best blending method was expected to be that which resulted in the smoothest profile in the blended area. We thus assessed the smoothness with which data were blended, and the ability of each method to eliminate fusion artifacts at the N60 transition line.

In order to conserve space, we will not go into methodological detail regarding the algorithms for any method but that which produced the most smoothly blended output, the Gaussian blend (Section 3.3). The Gaussian method blends the two DEMs via a weighted average in which the contribution of CGIAR-CSI SRTM v4.1 data is zero at the N60 transition line, and increases as a function of distance moving south away from N60 (Eq. (2.1)).

$$fused_{x,y} = \begin{cases} \mathrm{ASTERGDEM2}_{x,y} & \mathrm{above N60} \\ w_{x,y}\mathrm{ASTER}GDEM2_{x,y} + (1 - w_{x,y})\mathrm{CGIAR\text{-}CSISRTMv4.1}_{x,y} & \mathrm{below N60} \end{cases} \quad (2.1)$$

where $w_{x,y} = \exp(-\mathrm{r}D_y^2)$ and D_y is the distance from N60 in units of pixels.

We parameterized the algorithm using $r = 0.001$, in order to produce a blend zone that was neither unwieldy nor too narrow. This resulted in equal weights for CGIAR-CSI SRTM v4.1 and ASTER GDEM2 at a distance of ~2.3 km (26 latitudinal rows) south of the N60 transition line, and a relative weight for ASTER GDEM2 of only 1% by ~6.1 km (68 latitudinal rows) south of N60.

Following blending tests, we performed the Gaussian method for EarthEnv-DEM90 using smoothed 5° × 1° (longitude × latitude) tiles, spanning N59 to N60, from each of the pre-processed ASTER GDEM2 and CGIAR-CSI SRTM v4.1 datasets. For ASTER GDEM2 data, the production of blend zone input tiles is described in Section 2.2.1. For CGIAR-CSI SRTM v4.1 data, these tiles were clipped from 5° × 5° SRTM zone tiles (see Section 2.2.2). Blending was carried out using the raster package in R (Hijmans and van Etten, 2012; R Development Core Team, 2013).

Table 1
Statistical ranges for comparisons of real versus interpolated pixel values in simulated void areas across three test regions. Ranges were calculated at tensions of 110–135, and smoothing parameter values of 0.5, 0.6, and 0.7.

Test region	% Shared values	Correlation	RMSE
E. Russia	4.1–4.3	0.9779–0.9790	21.203–21.753
N. Central Canada	7.4–7.9	0.9744–0.9756	8.800–9.002
NW Canada	3.3–3.8	0.9877–0.9884	49.440–50.940

2.2.5. Accuracy assessments

After fully assembling EarthEnv-DEM90, and to evaluate of the overall quality of the dataset, we performed accuracy assessments in which we compared elevational values from EarthEnv-DEM90 and input DEM products to control points. We included three test areas, one in each of the ASTER, SRTM and blend zones. Accuracy assessments were performed using data from the anthropogenic and natural features dataset from the Global Elevation Data Testing Facility (GEDTF: http://www.gedtf.org/, 2013). This dataset (produced by a team led by Dr. Kazimierz Becek, at the Universiti of Brunei Darussalam) provides elevational measures for large, nearly-flat features, most of which are airport runways, around the globe. Individual measurements were mostly obtained using Google Earth, and then verified from the World Aeronautical Database, www.airnav.com, and other sites (http://www.gedtf.org/, 2013). We chose the GEDTF dataset because it covers a large spatial extent, and thus provides consistently obtained data points by which to assess DEM accuracy over multiple areas while minimizing additional error such as that introduced with the use of several control point datasets.

3. Results

The output ENO-90DEM covers ~91% of the global landmass, from latitudes S60 to N83. This omits Antarctica, where the only available data (ASTER GDEM2) contains such numerous, large voids (Urai et al., 2012) that we could not confidently improve the input data enough to be included in EarthEnv-DEM90. Results for all procedures and tests in the applicable data zones described above are as follows:

3.1. ASTER zone

In analyzing of best tension and smoothing parameter combinations for use during void-filling, we compared actual to rst interpolated pixel values for over 400 such combinations within the Eastern Russia, North-central Canada, and Northwestern Canada test regions. Results indicated that interpolated pixel estimates were effectively equivalent for tensions of 110–135 and smoothing of 0.5, 0.6 and 0.7 (Table 1), though the 135/0.6 combination performed slightly better than all others. This parameter combination

was then used during tests of the performance of the DSF method versus spline interpolation alone. For the North-central Canada test region, the DSF method estimated pixel values within simulated voids more accurately than did interpolation alone (RMSE: 8.176–8.800 and correlation: 0.9793–0.9756, for DSF versus interpolation, respectively). Following these analyses, we performed void-filling through the DSF method for all tiles containing voids in the ASTER zone, in order to obtain void-free tiles for EarthEnv-DEM90 (e.g. Fig. 5).

3.2. DEM smoothing

The adaptive multi-scale smoothing performed for all tiles in EarthEnv-DEM90 lead to a marked reduction in terrain noise in the output dataset, while having little impact on actual terrain variation (Fig. 6; Table 2). For example, EarthEnv-DEM90 elevational values over a 150-pixel (~13.5 km) latitudinal profile in a mountainous region of Alaska exhibited similar natural terrain variation to those of input ASTER GDEM2 data, but noticeably less noise (Fig. 6A). Here, the maximum difference between adjacent pixels was 179 m versus 194 m for EarthEnv-DEM90 and input ASTER GDEM2, respectively (Table 2). In addition, both the absolute mean and standard deviation of the absolute mean differences between adjacent pixels were smaller for EarthEnv-DEM90 than for input ASTER GDEM2 data (7.9–10.5 m, and 25.9–34.9; Table 2). This noise reduction was even more apparent in a test region near Western Australia's Lake Disappointment. Over a mere 50-pixel (~4.5 km) latitudinal profile, input CGIAR-CSI SRTM v4.1 data displayed significantly more noise than did smoothed EarthEnv-DEM90 data (Fig. 6B). This was substantiated by adjacent pixel comparisons across the latitudinal profile, for which input CGIAR-CSI SRTM v4.1 exhibited a maximum, absolute mean and standard deviation of absolute mean differences of 252 m, 34.9 m and 64.1, while those of EarthEnv-DEM90 were 140 m, 10.3 m, and 23.8 (Table 2).

From a visual perspective, the noise reduction achieved via multi-scale smoothing was easily seen in regions encompassing flat terrain or drainage channels, where land that appeared irregular in input DEMs became more level and smooth in EarthEnv-DEM90 (e.g. Fig. 7A and B). Noise reduction, however, was also apparent over uneven terrain. Here, elevational differences among pixels occupying changing slopes were markedly more defined in EarthEnv-DEM90 than in the input DEMs (Fig. 7C and D), as evidenced by topographical lines in EarthEnv-DEM90 that were obscured by terrain noise in input DEMs.

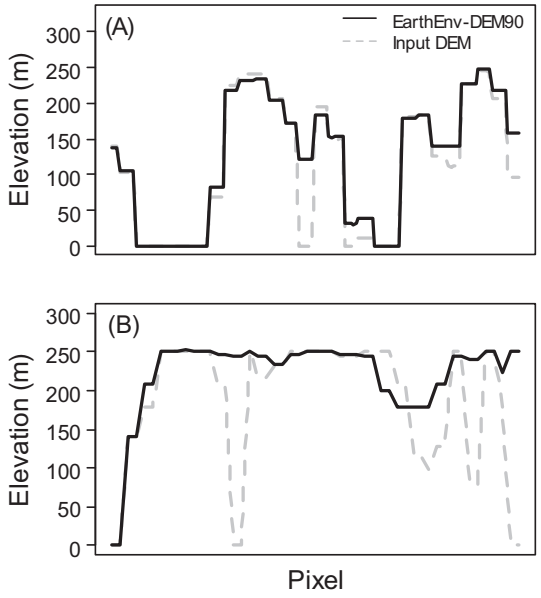

Fig. 6. Latitudinal profiles showing noise reduction over test areas in a mountainous region of Alaska (A) and near Western Australia's Lake Disappointment (B). Test regions encompass strips of 150 (Alaska) or 50 (Australia) pixels, and exhibit marked noise reduction in EarthEnv-DEM90 (black line) as opposed to input DEMs (dashed grey line).

3.3. Blend zone

Our analyses of the best method by which to combine ASTER GDEM2 and CGIAR-CSI SRTM v4.1 data at the N60 transition line revealed that these two datasets were too incongruous to be fused by simply mosaicking them together. In the region just south of N60, where both datasets were available, we found marked elevational bias between the two DEMs. For latitudinal profiles in our N59.875 to N60 test region, mean elevation was an average of 11.65 m higher in CGIAR-CSI SRTM v4.1 than in ASTER GDEM2 (Fig. 8A). CGIAR-CSI SRTM v4.1 also exhibited a uniformly shallower mean slope, by approximately ~1°, than did ASTER GDEM2 (Fig. 8B). These differences combined to produce further divergences in the other two measures analyzed, mean aspect and flow direction (results not shown). Because of these disparities, a sharp 'elevational cliff' and slope change were apparent when ASTER GDEM2 and CGIAR-CSI SRTM v4.1 data were simply fused at the N60 transition line (Fig. 8C and D).

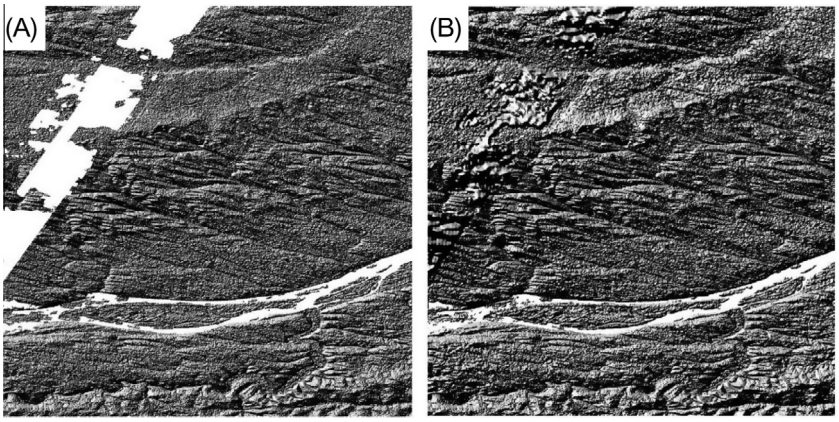

Fig. 5. Relief map of ASTER GDEM2 (A) and EarthEnv-DEM90 (B) data showing void-filling (ASTER GDEM is a product of METI and NASA). Example area spans latitudes N61 to N62, longitudes E128 to E129.

Table 2
Adjacent pixel comparisons for input DEM data versus smoothed EarthEnv-DEM90 over two test regions. The absolute mean difference (in meters), standard deviation (S.D.) of the absolute mean differences, and maximum difference (in meters) are provided for a mountainous area in Alaska (150-pixel test region) as well as an area near Australia's Lake Disappointment (50-pixel test region).

	Alaska test region		Australia test region	
	Input ASTER-2	EarthEnv-DEM90	Input SRTM-4	EarthEnv-DEM90
Absolute mean difference (m)	10.5	7.9	34.9	10.3
S.D. of mean differences	34.9	25.9	64.1	23.8
Maximum difference (m)	194	179	252	140

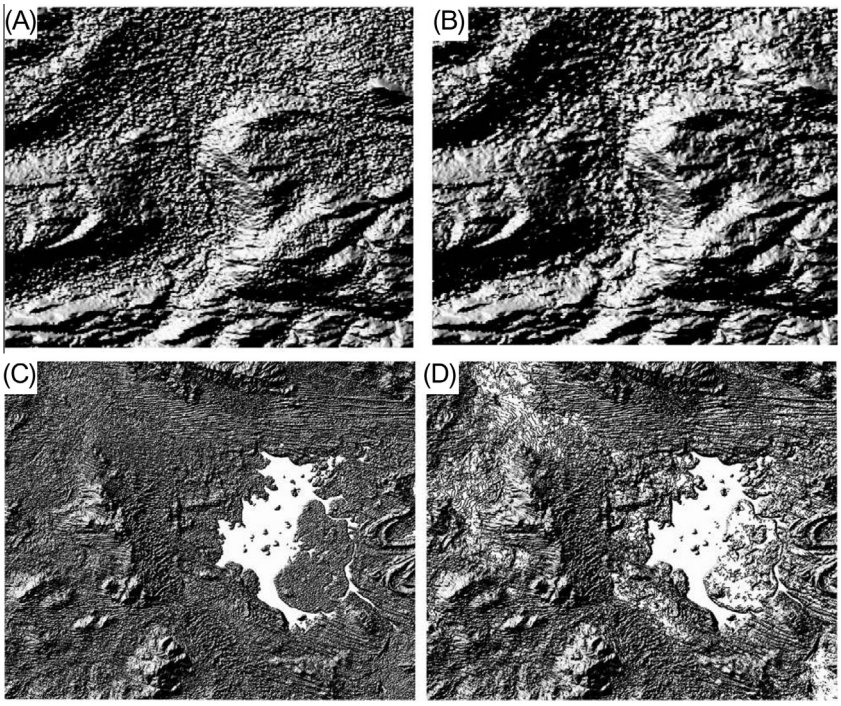

Fig. 7. Hillshade maps of input ASTER GDEM2 (A) or CGIAR-CSI SRTM v4.1 (C) data versus smoothed EarthEnv-DEM90 (B and D). The first example area comprises a mountainous region of Alaska (A and B) where smoothing (e.g. reduced graininess) is observed in drainage channels. The second example area encompasses a region surrounding Western Australia's Lake Dissapointment (C and D), where noise reduction is evident: (1) around the peak in the left-center of the image, where terrain contours that are distorted by noise in CGIAR-CSI SRTM v4.1 are visible on the slope leading up to the peak in EarthEnv-DEM90, and (2) on the salt flat at the east of the lake, which appears relatively flat in EarthEnv-DEM90 but is characterized by noisy terrain variation (graininess) in CGIAR-CSI SRTM v4.1.

Unfortunately, the elevational bias described above was not systematic across pixels in the ASTER GDEM2 and CGIAR-CSI SRTM v4.1 DEMs. In our test region, for example, various groups of pixels exhibited upper and lower quartiles of ~3 to ~20 m elevational differences, respectively, with up to 13 m spreads between quartiles. Similar results have been documented by other researchers (e.g. Wang et al., 2011), and this finding precludes the use of a constant correction factor by which one of the DEMs could otherwise be adjusted in order to produce smoothly fused data. Thus, we analyzed the effects of blending the datasets via weighted pixel averaging (Section 2.2.4).

Latitudinal profiles revealed that Gaussian weighted averaging eliminated the elevational cliff exhibited when the datasets were simply fused, and produced smoothly blended elevational values at the N60 transition line (Fig. 8E). In addition, Gaussian blending resulted in a smoother mean slope gradient (Fig. 8F) across the CGIAR-CSI SRTM v4.1/ASTER GDEM2 transition zone than did other blending methods (results not shown). This method was thus selected for blending ASTER GDEM2 and CGIAR-CSI SRTM v4.1.

3.4. Accuracy assessments

In the ASTER zone of EarthEnv-DEM90 we obtained GEDTF data for a 10° × 30° (latitude × longitude) test region in an area centering around Sweden (latitudes N60–70, longitudes E6–36). This relatively large test area was required in order to obtain enough control points for accuracy assessments in the generally data-poor northern latitudes. In all, we extracted data for 91 airports in this region. Each runway is associated with two elevational measurements (at the beginning and end of the runway), resulting in 182 total data points. The test region for the SRTM zone was smaller than that used in the ASTER zone, as more data were available in the more populated lower latitudes. Here, we obtained GEDTF data for a 10° × 10° test region (latitudes N33–43, longitudes W100–90), in the central plains of the United States. This area encompasses relatively flat terrain, the DEM accuracy of which is essential for many geophysical and biogeophysical applications. In addition, this area is more populated than most other flat regions of the globe, thus providing a large set of control points by which to assess DEM accuracy. In all, we extracted 484 control points (from 242 airports) in this test area. Finally, in the blend zone, there were 78 total control points (from 36 runways) available in the GEDTF dataset for the entire circumference of globe. Given this relatively small amount of data, we performed accuracy assessments using all control points in the N59 to N60 latitudinal band.

In the ASTER and SRTM zones, we anticipated that the accuracy of our new DEM product would be similar to that previously found for ASTER GDEM2 and CGIAR-CSI SRTM v4.1 (e.g. Rodriguez et al.,

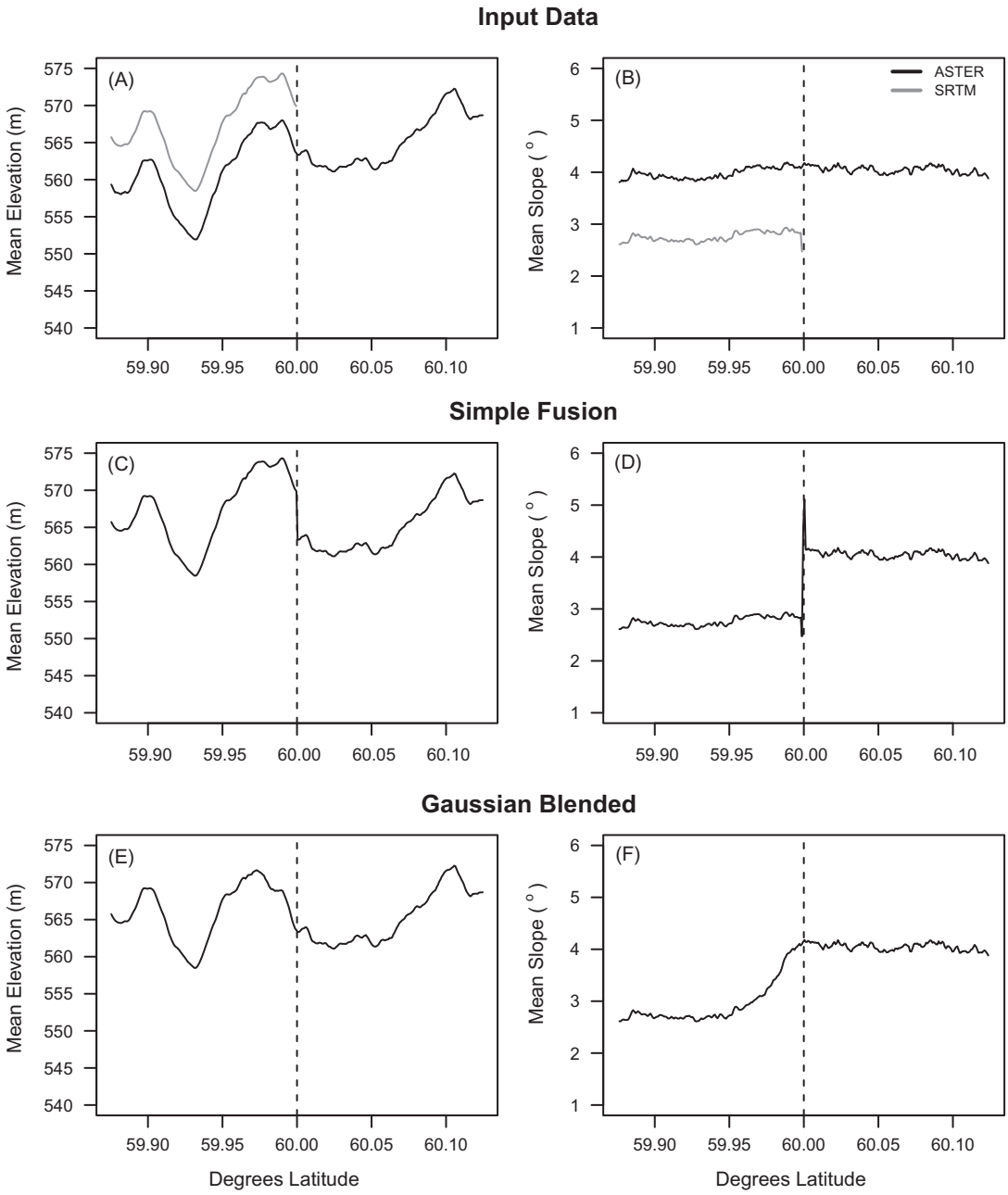

Fig. 8. Latitudinal profiles showing differences in mean elevation (A) and slope (B) for input CGIAR-CSI SRTM v4.1 (grey lie) and ASTER GDEM2 data (black line), and artifact elevational (C) and slope (D) changes that occur at the N60 transition line if the two datasets are simply fused as opposed to blended via Gaussian blending (E and F).

2005; Tachikawa et al., 2011; Li et al., 2012; Suwandana et al., 2012), given that the effects of multi-scale smoothing were typically small. This expectation was met in both regions. In the ASTER zone, both EarthEnv-DEM90 and ASTER GDEM2 elevational values were generally lower than were control point measurements (average differences of 6.2 and 5.8 m, respectively). Overall accuracy, however, was almost identical for the two datasets. Correlations between DEM and control point measurements were nearly perfect in both cases ($r_{180} = 0.998$), and RMSE's were extremely similar (10.554 and 11.178 for EarthEnv-DEM90 and ASTER GDEM2, respectively). The very slightly lower RMSE for EarthEnv-DEM90 was likely due to multi-scale smoothing induced improvements. Similarly, the accuracy of EarthEnv-DEM90 was almost identical to that of CGIAR-CSI SRTM v4.1 in the SRTM zone. Here, EarthEnv-DEM90 and CGIAR-CSI SRTM v4.1 measurements were an average of 1.64 and 1.66 m lower than were control points, respectively. Additionally, estimates from both DEMs were almost perfectly correlated with control point elevational values ($r_{482} = 0.999$ in both cases), and exhibited essentially the same RMSE (4.13 and 4.15 for EarthEnv-DEM90 and CGIAR-CSI SRTM v4.1, respectively).

For the blend zone accuracy assessment, we compared control point elevational values to those in EarthEnv-DEM90 and ASTER GDEM2. This allowed us to verify that the blending procedure produced more accurate measurements in this band than those seen in ASTER GDEM2, the input DEM that covers high northern latitudes. We found that EarthEnv-DEM90 elevational measures were an average of 0.82 m higher than were control point measurements, while ASTER GDEM2 data were an average of 3.08 m lower. EarthEnv-DEM90 measurements were also better correlated with control points ($r_{76} = 0.998$) than were ASTER GDEM2 values ($r_{76} = 0.982$). Finally, EarthEnv-DEM90 exhibited an approximately

three-fold lower RMSE compared to control points (5.362) than did ASTER GDEM2 (15.68).

4. Discussion and concluding remarks

4.1. EarthEnv-DEM90 – advances and opportunities

EarthEnv-DEM90 is a nearly-global grid of elevation estimates comprising DEM data sources that were previously available (at no-cost) for individual regions of the globe. This new compilation product combines the advantages the source DEMs (high quality of CGIAR-CSI SRTM v4.1, global coverage of ASTER GDEM2, high resolution of both) while also exhibiting a marked reduction in their pervasive data quality issues, due to rigorous quality-control techniques applied during EarthEnv-DEM90's creation. This is particularly true of the northernmost regions of the globe, where extensive data voids were filled from a combination of rigorously tested interpolation and information from an outside dataset. In addition, the application of the adaptive multi-scale smoothing method to the entire surface of EarthEnv-DEM90 led to a reduction in DEM noise. Finally, the blending of DEMs resulted in EarthEnv-DEM90 having a consistent transition across a surface that would otherwise have artifact elevational changes at the seam.

Although other researchers have produced fused DEM products, utilizing similar satellite-based DEM input data to those used for EarthEnv-DEM90 (Kääb, 2005; Karkee et al., 2008), these datasets have typically been created in order to enhance the quality of hydrography models and are thus limited to local or regional scales. Other, more far-reaching efforts are either not thoroughly described in terms of construction methodologies (e.g. Jonathan de Ferranti's 3 arc-sec product: http://www.viewfinderpanoramas.org/dem3.html, 2013), costly to users, or only available at coarse resolutions. The recently produced GMTED2010 (U.S. Geological Survey and National Geospatial-Intelligence Agency), for example, is a composited DEM product that is an improvement in both scale and accuracy (Carabajal et al., 2011) over older near-global products but that is only available at 7.5 arc-sec resolution. EarthEnv-DEM90 thus fills a product gap that currently exists for researchers that need high-resolution data in order to perform analyses in boreal or arctic areas, or those interested in macro-scale patterns and processes such as global water-flow (Oki and Sud, 1998), glacier retreat in the face of climate change (Scherler et al., 2008), species distributions for wide-ranging temperate species (Franklin, 1995; Braunisch et al., 2008), trans-continental infection risk and disease spread dynamics (Jentes et al., 2011), spatially explicit biogeochemical processes (e.g. Turner et al., 1996), etc.

4.2. EarthEnv-DEM90 – remaining limitations

Despite the marked advantages of EarthEnv-DEM90 compared to other products on the market today, the dataset is not without limitations. Most notably, the overarching data issues that are present in the ASTER GDEM2 and CGIAR-CSI SRTM v4.1 products, such as erroneous spikes and wells, carried through to EarthEnv-DEM90. This is because the adaptive multi-scale smoothing algorithm applied to EarthEnv-DEM90 was geared toward noise-reduction, not the correction of erratic and anomalous elevation values. This issue is especially prevalent in the ASTER zone of EarthEnv-DEM90. In addition, the finest resolution at which we could provide EarthEnv-DEM90 data was approximately 90 m, despite the obvious advantage of finer resolutions. In this regard, we were constrained by the combinations of resolution and quality exhibited by input datasets. For example, while ASTER GDEM2 is available at ~30 m resolution over global extents, quality control issues limit the utility of the present version. These issues include not only data voids, which is the focus here, but also shortcomings in general accuracy. For example, the vertical accuracy of ASTER GDEM2 varies from much better to distinctly worse than that of both CGIAR-CSI SRTM v4.1 and the previous version of ASTER GDEM, depending on study location (see Li et al., 2012; Suwandana et al., 2012). The accuracy of ASTER GDEM2 data is also reduced by the presence of substantial noise, which is even more apparent than in the previous product (Tachikawa et al., 2011). Given that such errors are multiplied when second-order products (e.g. slope and aspect grids) are derived from a DEM (Franklin, 1995), we chose to compromise resolution for quality in the construction of EarthEnv-DEM90.

5. Conclusions

We anticipate that higher resolution DEMs will become increasingly available to the public in the future, as updated (e.g. future versions of ASTER GDEM) and new products are released. Such products, however, require a still-lengthy period of quality control and assurance before being fit for use, even after initial release. In addition, even when proper QA/QC has been performed, a consistent challenge with DEM products is understanding exactly what processing steps have been taken to create new versions and new products. Here we believe that EarthEnvDEM-90 may have particular value, as much for the attention to describing the data as in the data itself. In particular, the methods we used to fill input DEM data voids, smooth the global surface, and assemble and fuse the input DEM products, are likely to be broadly applicable to the creation of new DEM datasets. These methods have been encoded into processing steps and working code that will be freely distributed to others upon request. Until other DEMs are available, with similar quality control, and similar levels of provenance and processing metadata, we think the EarthEnv-DEM90 will prove to be a very useful global DEM product for researchers performing a wide variety of research projects across several disciplines.

5.1. EarthEnv-DEM90 – availability and metadata

The EarthEnv-DEM90 dataset can be downloaded, in gzipped format, from one of two sources: an easy-access webpage (where users can select tiles of interest via a simple map or by entering a set of boundary coordinates) at: http://dem.earthenv.org/, or a data-hosting website at: http://mirrors.iplantcollaborative.org/earthenv_dem_data. The DEM comprises individual tiles that are $5^\circ \times 5^\circ$ or $5^\circ \times 3^\circ$ (longitude by latitude). Tiles are in EHdr format, are un-projected (spatially referenced to the WGS84 geodetic datum), and are 16-bit signed integer. Each tile is named to indicate its lower-left tile coordinate in degrees latitude and longitude. A binary dataset, EarthEnv-DEM90Void, can also be downloaded from the data-hosting website. This dataset comprises tiles that are of the same resolution and spatial extent as those in EarthEnv-DEM90, and that correspond to each EarthEnv-DEM90 tile in which voids were filled during processing (with no tile where void-filling was unnecessary). This dataset thus spatially distinguishes void-filled pixels from those containing primary data. It is worth noting that the values of many of these 'primary data' pixels may differ slightly between EarthEnv-DEM90 and the source dataset(s) due to the multiple processing steps by which raw data were blended and smoothed. Finally, we have also produced metadata documentation for EarthEnv-DEM90, so that it may be easily discoverable and any changes can be updated in ways that help users understand how it was created, and by whom. The metadata correspond to the EML dataset metadata standard, and is available as a comma delimited file at: http://mirrors.iplantcollabora-

tive.org/earthenv_dem_data. We recognize that provision of metadata in alternative formats, such as those corresponding to FGDC and GCMD DIF standards, would further enhance discovery in national and international repositories, and such efforts will be undertaken in future EarthEnv-DEM90 updates.

Acknowledgements

This work was conducted as a part of the Environment and Organisms (ENO) Working Group supported by the National Center for Ecological Analysis and Synthesis, a Center funded by NSF (Grant #EF-0553768), the University of California, Santa Barbara, and the State of California. Key additional ENO team members are: Walter Jetz, Brian McGill, Martha Narro, Adam Wilson, Mao-Ning Tuanmu, Benoit Parmentier, Mark Schildhauer, and George Cooper. Additional funding was supplied by the National Aeronautics and Space Administraion (NASA) Grant #NNX11AP72G. The input DEMs acquired for this project were obtained from the following sources: ASTER GDEM2 were obtained through the online Data Pool at the NASA Land Processes Distributed Active Archive Center (LP DAAC), USGS/Earth Resources Observation and Science (EROS) Center, Sioux Falls, South Dakota (https://www.lpdaac.usgs.gov/get_data); CGIAR-CSI SRTM v4.1 were obtained online through the CGIAR-CSI download database at http://srtm.csi.cgiar.org/; GLSDEM were obtained online through the GLCF FTP server at http://glcf.umd.edu/data/glsdem/.

We are particularly grateful to John Gallant for contributing the multi-scale smoothing algorithm that was used during the production of EarthEnv-DEM90, as well as continuous support and feedback during its implementation. We also thank past ENO working-group members that include (but are not limited to) Yuina Nunokawa, Rick Reeves, John Donahue, and others. Additionally, we appreciate the input of two anonymous reviewers, whose comments resulted in major improvements to this manuscript. Finally, we thank the iPlant Collaborative team for hosting EarthEnv-DEM90 and for facilitating the countless meetings of minds without which this project would not have been feasible. The iPlant Collaborative is funded by a grant from the National Science Foundation (#DBI-0735191). URL: http://iplantcollaborative.org.

References

Braunisch, V., Bollmann, K., Graf, R.F., Hirzel, A.H., 2008. Living on the edge-modelling habitat suitability for species at the edge of their fundamental niche. Ecological Modelling 214 (2), 153–167.

Burt, P.J., Adelson, E.H., 1983. A multiresolution spline with application to image mosaics. ACM Transactions on Graphics 2 (4), 217–236.

Carabajal, C.C., Harding, D.J., Boy, J.P., Danielson, J.J., Gesch, D.B., Suchdeo, V.P., 2011. Evaluation of the global multi-resolution terrain elevation data 2010 (GMTED2010) using ICESat geodetic control. In: International Symposium on Lidar and Radar Mapping Technologies. International Society for Optics and Photonics, pp. 82861Y–82861Y.

Farr, T.G., Rosen, P.A., Caro, E., Crippen, R., Duren, R., Hensley, S., Kobrick, M., Paller, M., Rodriguez, E., Roth, L., Seal, D., Shaffer, S., Shimada, J., Umland, J., Werner, M., Oskin, M., Burbank, D., Alsdorf, D., 2007. The shuttle topography mission. Reviews of Geophysics 45 (2).

Fisher, P.F., Tate, N.J., 2006. Causes and consequences of error in digital elevation models. Progress in Physical Geography 30 (4), 467–489.

Franklin, J., 1995. Predictive vegetation mapping: geographic modelling of biospatial patterns in relation to environmental gradients. Progress in Physical Geography 19 (4), 474–499.

Gallant, J.C., 2011. Adaptive smoothing for noisy DEMs. Geomorphometry Conference, Redlands, CA, 7–9 September. (Published at: <http://geomorphometry.org/Gallant2011>).

Gesch, D., Oimoen, M., Zhang, Z., Danielson, J., Meyer, D., 2011. Validation of the ASTER Global Digital Elevation Model (GDEM) Version 2 over the Conterminous United States (USGS Validation Report), <http://www.ersdac.or.jp/GDEM/ver2Validation/Appendix_B_CONUS%20_GDEMv2_validation_report.pdf> (accessed 19.09.13).

Global Land Survey Digital Elevation Model (GLSDEM) Technical Guide, <http://www.glcf.umd.edu/library/guide/techguide_glsdem.pdf> (accessed 06.05.13).

Grohman, G., Kroenung, G., Strebeck, J., 2006. Filling SRTM voids: the delta surface fill method. Photogrammetric Engineering and Remote Sensing 72 (3), 213–216.

Hargrove, W.W., 1995. Interpolation of rainfall in Switzerland using a regularized spline with tension. <http://www.geobabble.org/~hnw/sic97/> (accessed 20.09.13).

Hijmans, R.J., van Etten, J., 2012. Raster: Geographic data analysis and modeling. R package, version 2.0-41. <http://CRAN.R-project.org/package=raster>.

Hofierka, J., Parajka, J., Mitasova, H., Mitas, L., 2002. Multivariate interpolation of precipitation using regularized spline with tension. Transactions in GIS 6 (2), 135–150.

Hong, S.H., Jung, H.S., Won, J.S., 2006. Extraction of ground control points (GCPs) from synthetic aperture radar images and SRTM DEM. International Journal of Remote Sensing 27 (18), 3813–3829.

Jarvis A., Reuter, H.I., Nelson, A., Guevara, E., 2008. Hole-filled seamless SRTM data V4, International Centre for Tropical Agriculture (CIAT), <http://srtm.csi.cgiar.org> (accessed 23.05.13).

Jentes, E.S., Poumerol, G., Gershman, M.D., Hill, D.R., Lemarchand, J., Lewis, R.F., Staples, J.E., Tomori, O., Wilder-Smith, A., Monath, T.P., 2011. The revised global yellow fever risk map and recommendations for vaccination, 2010: consensus of the Informal WHO Working Group on Geographic Risk for Yellow Fever. The Lancet Infectious Diseases 11 (8), 622–632.

Kääb, A., 2005. Combination of SRTM3 and repeat ASTER data for deriving alpine glacier flow velocities in the Bhutan Himalaya. Remote Sensing of Environment 94 (4), 463–474.

Karkee, M., Steward, B.L., Abd Aziz, S., 2008. Improving quality of public domain digital elevation models through data fusion. Biosystems Engineering 101 (3), 293–305.

Li, P., Shi, C., Li, Z., Muller, J.-P., Drummond, J., Li, X., Li, T., Li, Y., Liu, Jingnan, 2012. Evaluation of ASTER GDEM VER2 using GPS measurements and SRTM VER4.1 in China. ISPRS Annals of the Photogrammetry, Remote Sensing and Spatial Information Sciences 22 (Parts 1-4), 181–186.

Mitasova, H., Mitas, L., 1993. Interpolation by regularized spline with tension: I. Theory and implementation. Mathematical Geology 25 (6), 641–655.

Mitasova, H., Mitas, L., Harmon, R.S., 2005. Simultaneous spline approximation and topographic analysis for Lidar elevation data in open-source GIS. IEEE Geoscience and Remote Sensing Letters 2 (4), 375–379.

NASA Land Processes Distributed Active Archive Center (LP DAAC). ASTER GDEM2, USGS/Earth Resources Observation and Science (EROS) Center, Sioux Falls, South Dakota, 2011.

Nikolakopoulos, K.G., Tsombos, P.I., Zervakou, A., 2007. Evaluating SRTM and ASTER DEM accuracy for the broader area of Sparti, Greece. Proc. Remote Sensing. International Society for Optics and Photonics, pp. 67460F–67460F.

Oki, T., Sud, Y.C., 1998. Design of total runoff integrating pathways (TRIP) – a global river channel network. Earth Interactions 2 (1), 1–36.

R Core Team, 2013. R: A language and environment for statistical computing. R Foundation for Statistical Computing, Vienna, Austria. ISBN 3-900051-07-0. <http://www.R-project.org/>.

Rodriguez, E., Morris, C.S., Belz, J.E., Chapin, E.C., Martin, J.M., Daffer, W., Hensley, S., 2005. An assessment of the SRTM topographic products. (Jet Propulsion Laboratory Technical Report). <http://www2.jpl.nasa.gov/srtm/SRTM_D31639.pdf> (accessed 19 September, 2013).

Scherler, D., Leprince, S., Strecker, M.R., 2008. Glacier-surface velocities in alpine terrain from optical satellite imagery – accuracy improvement and quality assessment. Remote Sensing of Environment 112 (10), 3806–3819.

Schindler, K., Papasaika, H., Schautz, S., Baltsavias, E., 2011. Improving wide-area DEMs through data fusion – chances and limits. Proceedings of the Photogrammetric Week 11, 159–170.

Suwandana, E., Kawamura, K., Sakuno, Y., Kustiyanto, E., Raharjo, B., 2012. Evaluation of ASTER GDEM2 in comparison with GDEM1, SRTM DEM and topographic-map-derived DEM using inundation area analysis and RTK-dGPS data. Remote Sensing 4 (8), 2419–2431.

Tachikawa, T., Kaku, M. Iwasaki, A., Gesch, D., Oimoen, M., Zhang, Z., Danielson, J., Krieger, T., Curtis, B., Haase, J., Abrams, M., Crippen, R., Carabajal, C., 2011. ASTER Global Digital Elevation Model Version 2 – Summary of Validation Results. (ASTER GDEM Validation Team Report). <https://lpdaacaster.cr.usgs.gov/GDEM/Summary_GDEM2_validation_report_final.pdf> (accessed 19.09.13).

Turner, D.P., Dodson, R., Marks, D., 1996. Comparison of alternative spatial resolutions in the application of a spatially distributed biogeochemical model over complex terrain. Ecological Modeling 90 (1), 53–67.

Urai, M., Tachikawa, T., Fujisada, H., 2012. Data acquisition strategies for ASTER global DEM generation. ISPRS Annals of the Photogrammetry, Remote Sensing and Spatial Information Sciences 22 (Parts 1–4), 199–202.

USGS, 2008. GLSDEM. Global Land Cover Facility, University of Maryland, College Park, Maryland.

Wang, L., Chen, J., Zhang, H., Chen, L., 2011. Difference analysis of SRTM C-band DEM and ASTER GDEM for global land cover mapping. Image and Data Fusion (ISIDF), 2011 International Symposium. IEEE, pp. 1–4.